Age-structured impact of social distancing on the COVID-19 epidemic in India

Rajesh Singh[1,*] and R. Adhikari[1,2,†]

[1] *DAMTP, Centre for Mathematical Sciences, University of Cambridge, Wilberforce Road, Cambridge CB3 0WA, UK*
[2] *The Institute of Mathematical Sciences-HBNI, CIT Campus, Chennai 600113, India*

The outbreak of the novel coronavirus, COVID-19, has been declared a pandemic by the WHO. The structures of social contact critically determine the spread of the infection and, in the absence of vaccines, the control of these structures through large-scale social distancing measures appears to be the most effective means of mitigation. Here we use an age-structured SIR model with social contact matrices obtained from surveys and Bayesian imputation to study the progress of the COVID-19 epidemic in India. The basic reproductive ratio $\mathcal{R}_0$ and its time-dependent generalization are computed based on case data, age distribution and social contact structure. The impact of social distancing measures - workplace non-attendance, school closure, lockdown - and their efficacy with duration is then investigated. A three-week lockdown is found insufficient to prevent a resurgence and, instead, protocols of sustained lockdown with periodic relaxation are suggested. Forecasts are provided for the reduction in age-structured morbidity and mortality as a result of these measures. Our study underlines the importance of age and social contact structures in assessing the country-specific impact of mitigatory social distancing.

I. INTRODUCTION

The novel coronavirus, COVID-19, originated in Wuhan and has spread rapidly across the globe. The World Health Organization has declared it to be a pandemic. In the absence of a vaccine, social distancing has emerged as the most widely adopted strategy for its mitigation and control [1]. The suppression of social contact in workplaces, schools and other public spheres is the target of such measures. Since social contacts have a strong assortative structure in age, the efficacy of these measures is dependent on both the age structure of the population and the frequency of contacts between age groups across the population. As these are geographically specific, equal measures can have unequal outcomes when applied to regions with significantly differing age and social contact structures. Quantitative estimates of the impact of these measures in reducing morbidity, peak infection rates, and excess mortality can be a significant aid in public-health planning. This requires mathematical models of disease transmission that resolve age and social contact structures.

In this paper we present a mathematical model of the spread of the novel coronavirus that takes into account both the age and social contact structure [2]. We use it to study the impact of the most common social distancing measures that have been initiated to contain the epidemic in India: workplace non-attendance, school closure, "janata curfew" and lockdown, the latter two of which attempt, respectively, complete cessation of public contact for brief and extended periods. We emphasise that models that do not resolve age and social contact structure cannot provide information on the differential impact of each of these measures. This information is vital since each of the specific social distancing measures have widely varying economic costs. Our model allows for the assessment of the differential impact of social distancing measures. Further, both morbidity and mortality from the COVID-19 infection have significant differences across age-groups, with mortality increasing rapidly in the elderly. It is necessary therefore to estimate not only the total number of infections but also how this number is distributed across age groups Our model allows for the assessment of such age-structured impacts of social distancing measures.

The remainder of our study is organized as follows. In Section (II) we compare the age and social contact structure of the Indian, Chinese, and Italian populations. Age distributions are sourced from the Population Pyramid website [3] and social contact structures from the state-of-the-art compilation of Prem et. al. [2] obtained from surveys and Bayesian imputation. We show that even with equal probability of infection on contact, the differences in age and social contacts in these three countries translate into differences in the basic reproductive ratio $\mathcal{R}_0$. In Section (III) we study the progress of the epidemic in the absence of any mitigation to provide a baseline to evaluate the effect of mitigation. In Section (IV) we investigate the effect of social distancing measures and find that the three-week lockdown that commenced on 25th March 2020 is of insufficient duration to prevent resurgence. Alternative protocols of sustained lockdown with periodic relaxation can reduce the infection to levels where social contact tracing and quarantining may become effective. Estimates of the reduction in morbidity and mortality due to these measures are provided. We conclude with a discussion on the possibilities and limitations of our study. An appendix provide details of our mathematical model and the social contact structure.

It has been known from retrospective analyses of the 1918–19 pandemic that delays in introducing social distancing measures are correlated with excess mortality [4, 5]. Our study confirms the urgency and need for sustained application of mitigatory social distancing.

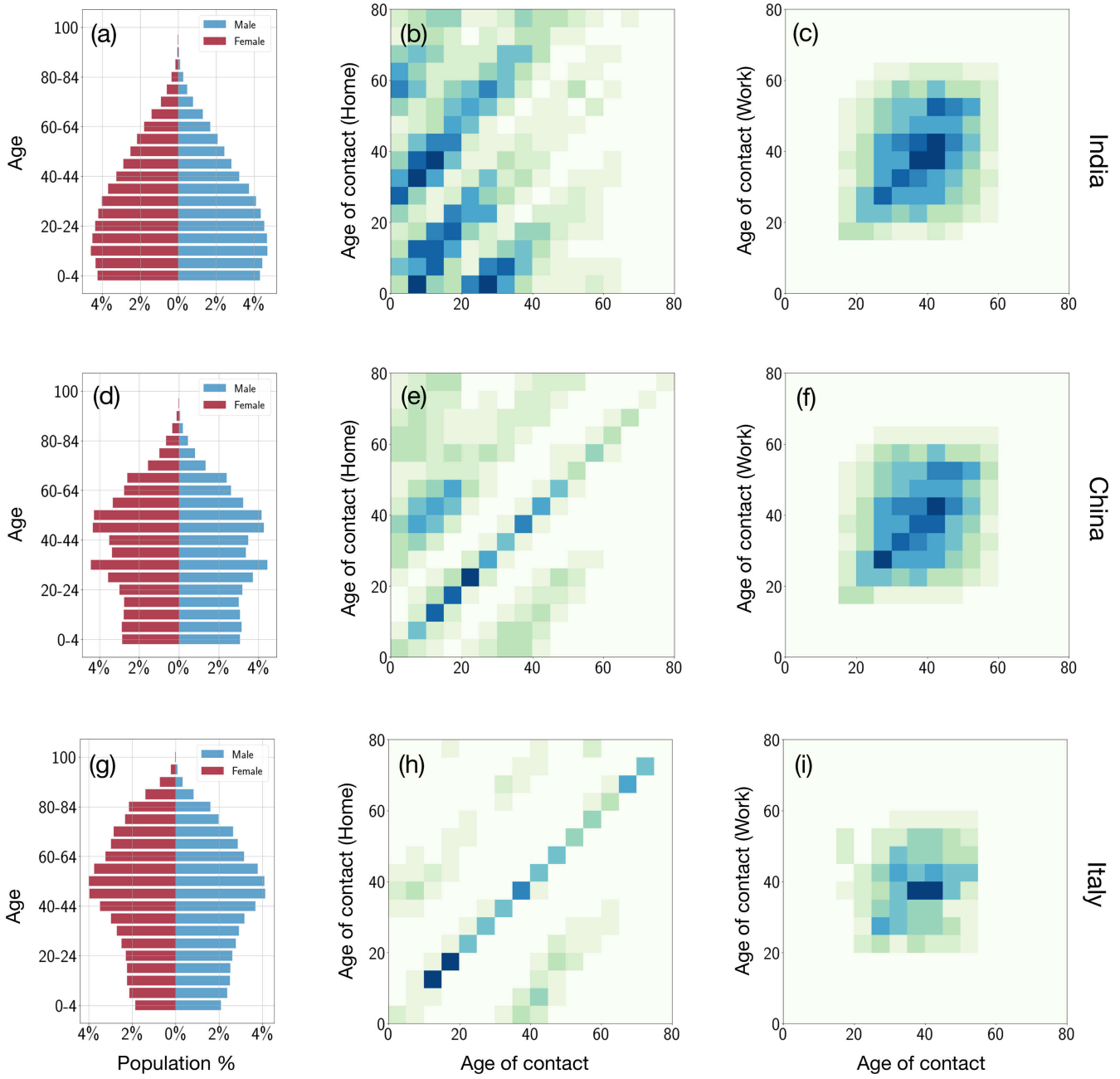

Figure 1. **Age and contact structures of the populations of India, China and Italy**. The first column shows population pyramids by age and gender. The second and third columns show the contact structures in households and workplaces with darker colours representing greater contacts. The diagonal dominance of these matrices shows strong assortative mixing in all three countries. Significant differences appear in the off-diagonals. In India, the pentadiagonal character of the household contacts reflects the prevalance of three-generation households, which are smaller in China and negligible in Italy.

II. AGE AND CONTACT STRUCTURES

In Fig.(1) we compare the age and contact structures of the populations of India, China and Italy. The aim of this comparison is to highlight their differences and to emphasise the effect these have on the spread of an infectious disease. Panels (a), (d) and (g) show the fraction of the population (separated by gender) in five-year age groups terminating at the age of eighty. The Taj Mahal dome shape of the Indian age distribution is typical of those undergoing a demographic transition. The narrower base of both Chinese and Italian populations is typical of aging populations at or near sub-replacement fertility. Panels (b), (e) and (h) show the contact between age groups in the household setting, represented by matrices C_{ij}^{H} where darker squares indicate larger con-

Country	Basic reproductive ratio
India	$\mathcal{R}_0 = 136\beta$
China	$\mathcal{R}_0 = 117\beta$
Italy	$\mathcal{R}_0 = 119\beta$

Table I. **Country-specific basic reproductive ratio** of the age-structured SIR model for fixed probability of infection on contact β and $\gamma = 1/7$ (see text). The difference between countries is attributed to their differing age and social contact structures.

tacts. As noted in [2], the features common to all three are the diagonal dominance, reflecting contact *within* age groups (*i.e.* siblings and partners) and the prominent off-diagonals, separated by the mean inter-generation gap, reflecting contacts *between* age groups (*i.e.* children and parents). The principal difference in India is the presence of a third dominant diagonal, again separated by the mean inter-generation gap, reflecting the prevalence of three-generation households. This quantifies the significant contact between children and grand-parents and the possibility of substantial of transmission of contagion from third to first generations. Such contacts are smaller in China and negligible in Italy. Panels (c), (f) and (i) show the contact C_{ij}^W between age groups in the workplace. In contrast to households, the work contact patterns are more homogeneous across age groups in all three countries, indicating that the workplace contributes to the transmission of contagion between age groups that are, otherwise, largely separated from each other in the household. The boundaries of these age groups are larger in India and China than in Italy. The matrices C_{ij}^S for schools (shown for India in the appendix) are strongly assortative, with primary contacts within the school-going ages and smaller contacts between age groups reflecting student-teacher interactions. The matrices C_{ij}^O for other spheres of contact (shown for India in the appendix) are strongly assortative, reflecting the preferential social contact within age groups in this sphere, but otherwise do not show systematic patterns. In summary, then, in India the home provides the main channel of transmission between three generations, the workplace provides the main channel of (largely homogeneous) transmission between working age groups, the school the main channel of transmission within children and to a smaller extent between children and adult teachers, while other spheres of contact, due to the assortative mixing, contribute to transmission within age groups.

Do these differences have a quantitative impact on the transmission of disease? We answer this affirmatively by comparing the basic reproductive ratio $\mathcal{R}_0$ for each of these populations for an infectious disease with identical probability of infection on contact β and rate of recovery γ for the age-structured SIR model described in Appendix 1. These differences underline the importance of resolving the age and social contact structure of a population when forecasting the progress of an infection and the impact of social distancing measures. With this background, we now turn to our forecast for the progress of the COVID-19 epidemic in India.

III. EPIDEMIC WITHOUT MITIGATION

We fit our mathematical model, described in detail in Appendix, to case data to estimate the probability of infection on contact β. Though our model allows for infectives to be both asymptomatic and symptomatic, given the large uncertainty in estimating asymptomatic cases, we assume all cases to be symptomatic. A possible effect of this is to underestimate the severity of the outbreak. We then run the model forward in time to forecast the progress of the epidemic with results shown in Fig. (2). Panel (a) shows the fit to case data available upto 25th March 2020 and a three-week forecast, *in the absence* of social distancing measures. The basic reproductive ratio is $\mathcal{R}_0 = 2.10$. Panel (b) shows a five month forecast, again, in the absence of social distancing. The peak infection is reached at the end of June 2020 with in excess of 150 million infectives. The total number infected is estimated to be 900 million. Panel (c) shows the time-dependent effective basic reproductive ratio $\mathcal{R}_0^{\text{eff}}(t)$ which gives the dominant contribution to the linearised growth at any point in time. This number is greater than unity before peak infection and smaller than unity beyond peak infection. The serves as a useful measure of the local rate of change of infectives at any point in time. In Fig. (3) we provide estimates of (a) the morbidity and (b) the excess mortality from the unchecked spread of the epidemic. The fraction infected across age groups is the largest for the 15-19 year olds and least amongst the 75-79 year olds. However, due to the strong age-dependence in death rates, mortality is amongst the least for the 15-19 year olds and greatest for the 60-64 year olds. We emphasise that these numbers, alarming as they are, are counterfactuals, as mitigation measures are already in place of this writing. They do, however, point to the unbearable cost in human life that must be paid for the any lack of, or delay in, mitigatory action.

IV. IMPACT OF SOCIAL DISTANCING

We now investigate the impact of social distancing measures on the unmitigated epidemic. We assume that social distancing in any public sphere, which in our model is partitioned into workplace, school and all others, removes all social contacts from that sphere. This, of course, transfers the weight of these removed contacts to the household, where people must now be confined.

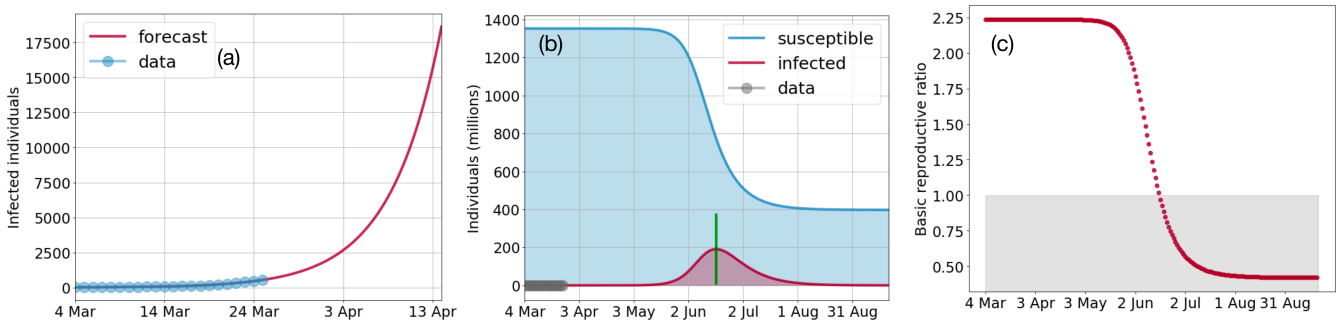

Figure 2. **Forecast of the COVID-19 epidemic in India without mitigatory social distancing.** Panel (a) shows the number of confirmed cases of till 25th March 2020 (blue circles) and three-week forecast (red line) from a fit of our model. Panel (b) extends this forecast to 5 months showing the number of infectives (red) and the number of susceptibles (blue). In the absence of mitigation, an expected 0.9 billion people would be infected in total, with a peak infection of 190 million people in 105 days as indicated by the green bar. Panel (c) shows the effective basic reproductive ratio $\mathcal{R}_0^{\rm eff}(t)$ as a function of time. This reduces to below unity beyond the peak infection. This forecast assumes all cases to be symptomatic so $\bar{\alpha} = 1$. The fit parameter $\beta = 0.0165$ and we set $\gamma = 1/7$ [1].

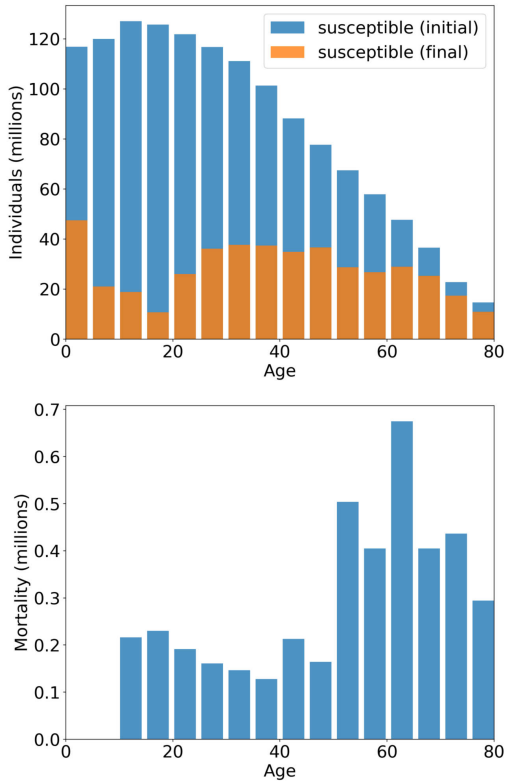

Figure 3. **Estimates of morbidity and mortality without mitigatory social distancing.** The top panel shows the distribution across age groups of the number of susceptibles at the start of the epidemic (blue bars) and at the end of the five month forecast (orange bars). Their difference is the total number infected in that five month period. Greatest infection is seen amongst the 15-19 year olds and least amongst the 74-79 year olds. The bottom panel shows the number of mortalities which, due to the strong age-dependence, is not proportional to the number of infections. The parameters for these estimates are identical to those in Fig. (2).

We ignore this in the first instance. We interpret the lockdown imposed from 25th March 2020 to remove *all* social contacts other than the household ones. This is an optimistic interpretation but it does allow us to assess the most favourable impact of such a measure. The results that follow, then, are an expected best-case scenarios. Then, the time-dependent social contact matrix at time t is

$$C_{ij}(t) = C_{ij} - u(t)(C_{ij}^W + C_{ij}^S + C_{ij}^O) \qquad (1)$$

where $C_{ij} = C_{ij}^H + C_{ij}^W + C_{ij}^S + C_{ij}^O$ is the sum of all social contacts comprising of contributions from the household, workplace, schools and all others, with obvious superscripts. The control function, described in Appendix, is constructed to reflect a social distancing measure that is initiated at $t = t_{\rm on}$ and suspended at $t = t_{\rm off}$. The measure has a lag t_w to be effective which we choose to be shorter than a day. The function varies smoothly from zero to one in the window $t_{\rm on} - t_{\rm off}$. For repeated initiations and suspensions, the control function is a sum of such terms with times adjusted accordingly. It is possible, of course, to have differentiated controls which apply distinct social distancing measures at different times and for different durations. We do not explore these here as the general setting for such an investigation would be within the framework of optimal control theory [6] with an appropriate cost function. We postpone this to future work.

Our results are show in in the four panels of Fig. (4) for four different control protocols. Panel (a) shows the effect of the three-week lockdown. While this immediately changes the sign of the rate of change of infectives, it does not reduce their number sufficiently to prevent a resurgence at the end of the lockdown period. Panel (b) shows the effect a suspension of the lockdown by 5 days followed by a further lockdown of 28 days. This too, does not reduce the number of infectives sufficiently to

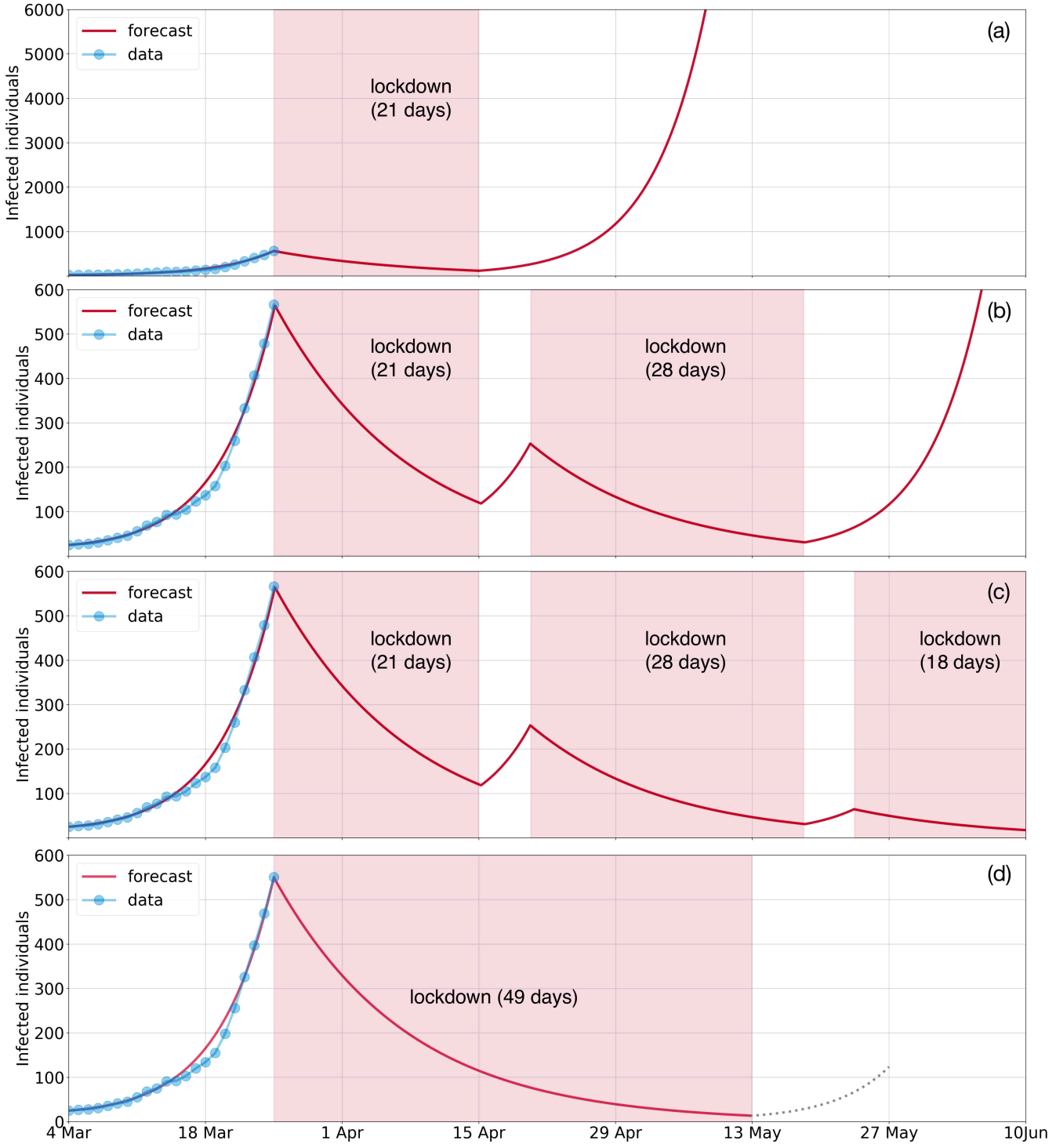

Figure 4. **Forecast of the COVID-19 epidemic in India with mitigatory social distancing.** Each of the four panels shows the variation in the number of infectives with lockdowns of various durations. The three-week lockdown starting 25th March does not prevent resurgence after its suspension as shown in panel (a). Neither does a further lockdown of 28 days spaced by a 5 day suspension, shown in panel (b). The protocols in panels (c) and (d), comprising of three lockdowns with 5 day relaxations and a single 49 day lockdown reduce case numbers below 10. This forecast is based on all cases being symptomatic so $\bar{\alpha} = 1$. The fit parameter is $\beta = 0.0165$ and we set $\gamma = 1/7$ [1].

	Case 1	Case 2	Case 3	Case 4
Mortality	251	17	17	7

Table II. **Estimates of mortality in a 49 day window from 25th March with mitigatory social distancing.** Cases 1 through 4 correspond, respectively, to panels (a) through (d) of Fig.4. The parameters are identical to those in Fig. (4).

prevent resurgence. Panel (c) shows a protocol of three consecutive lockdowns of 21 days, 28 days and 18 days spaced by 5 days of suspension. This brings the number of infective below 10 where explicit contact tracing followed by quarantine may be successful in preventing a resurgence. Panel (d) shows a single lockdown period to reach the same number of infectives which our model predicts to be 49 days.

Table (II) show the excess mortality that can be expected for each of the social distancing measures above. While we emphasise, again, that these are likely to be best-case scenarios, the substantive message is that of the crucial importance of rapid and sustained social distancing measures in reducing morbidity and mortality.

V. DISCUSSION AND CONCLUSION

We have presented a mathematical model of the spread of infection in a population that structured by age and social contact between ages. Since contagion spreads through the structure of social contacts and the latter varies with age, it is necessary to resolve both these aspects of a population in any model that attempts to understand and predict how the modification of the social contact structure through social distancing impacts the spread of disease. Such models become useful when reliable estimates of contact structures are available. We have combined our mathematical model with the state-of-the-art contact structure compilation of Prem et. al. [2] and empirical case data available till the 25th March 2020 to assess the impact of social distancing measures in the spread of the COVID-19 epidemic in India. Our principal conclusion is that the three-week lockdown will be insufficient. Our model suggests sustained periods of lockdown with periodic relaxation will reduce the number of cases to levels where individualised social contact tracing and quarantine may become feasible.

Our mathematical model contains both asymptomatic and symptomatic infectives. Due to the paucity of data on the number of asymptomatic cases we have chosen to set these to zero. This provides a lower bound on the number of morbidities and mortalities and the intensity and duration of the social distancing measures that are required for mitigation. Extensive testing of the population can provide data on the number of asymptomatic cases and this, when incorporated into our model, will provide more accurate estimates of the progress of the epidemic and the impact of mitigatory social distancing. More generally, there are uncertainties in all parameters of our model and these would translate into uncertainties in forecasts and estimates. These uncertainties can be reduced with better availability of case data and the uncertainties can be quantified through Bayesian error propagation analysis. The principal regional differences in India appear to be in the time of initiation of the infection and for the cases to reach the critical size where community transmission begins. Though our model is not spatially resolved, it can be applied region-wise by fitting it to regional case data.

In closing, we issue the necessary caveats. To quote G. P. Box, "Since all models are wrong the scientist must be alert to what is importantly wrong. It is inappropriate to be concerned about mice when there are tigers abroad" [7]. The three components of our study involve the mathematical model, the sources of data, and the numerical code. We have provided an explicit description of our mathematical model, our data sources are referenced, and our numerical implementation is open-sourced. We take these to be essential desiderata for modeling to inform policy. The mathematical model of an infection can aid in qualitative understanding and quantitative prediction but it should not be used in isolation from other perspectives, including economic, medical, social and ethical ones.

R.S. acknowledges the support of a Royal Society-SERB Newton International Fellowship. RA thanks colleagues at King's College, Cambridge for their encouragement and forbearance while this work was being completed.

APPENDIX A: MATHEMATICAL MODEL

Epidemiological model: We consider a population aggregated by age into M groups labelled by $i = 1, 2, \ldots M$. The population within age group i is partitioned into susceptibles S_i, asymptomatic infectives I_i^a, symptomatic infectives I_i^s and removed individuals R_i. The sum of these is the size of the population in age group i, $N_i = S_i + I_i^a + I_i^s + R_i$ [8–11]. We ignore vital dynamics and the change in age structure on the time scale of the epidemic. Therefore each N_i and, consequently, the total population size

$$N = \sum_{i=1}^{M} N_i \tag{2}$$

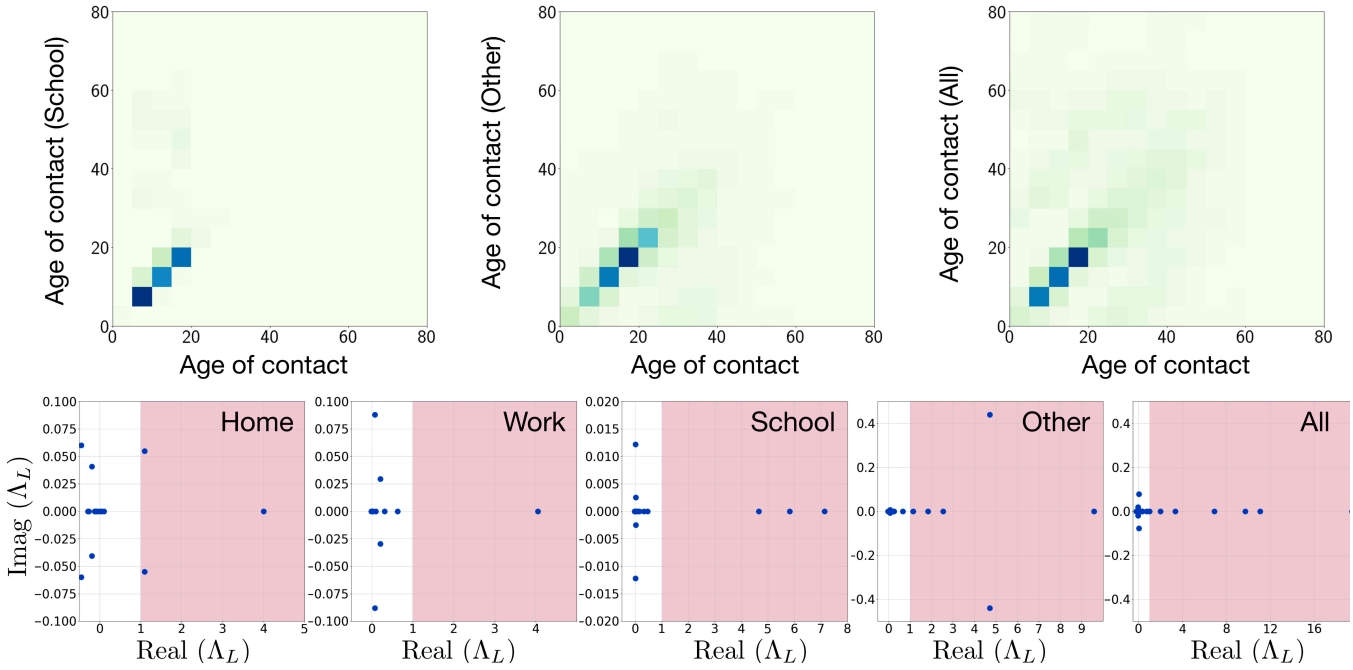

Figure 5. **Contact structures of the Indian population and their eigenspectrum.** The first two figures in the top row show the contact structure in India in schools and other locations respectively. This completes the partial list of contact structures in India shown in Fig.1. The third figure shows the sum of all contacts. The large number of contacts of 15-19 year olds is consistent with their greatest rate of infection, show in in Fig. (3). The second rows show the eigenvalue of the $\boldsymbol{L}$ matrix for $\bar{\alpha} = \beta = \gamma = 1$. The magnitude of the largest eigenvalue determines the basic reproductive ratio. The eigenanalysis helps estimate this quantity for each of the structures contributing to social contacts.

remain constant in time. We assume that the rate of infection of a susceptible individual in age group i is

$$\lambda_i(t) = \beta \sum_{j=1}^{M} \left(C_{ij}^a \frac{I_j^a}{N_j} + C_{ij}^s \frac{I_j^s}{N_j} \right), \quad i, j = 1, \dots M \quad (3)$$

where β is the probability of infection on contact (assumed intrinsic to the pathogen) and C_{ij}^a and C_{ij}^s are, respectively, the number of contacts between asymptomatic and symptomatic infectives in age-group j with susceptibles in age-group i (reflecting the structure of social contacts). We take the age-independent recovery rate γ to be identical for both asymptomatic and symptomatic individuals whose fractions are, respectively, α and $\bar{\alpha} = 1-\alpha$. With these assumptions the progress of the epidemic is governed by the age-structured SIR model

$$\begin{aligned} \dot{S}_i &= -\lambda_i(t) S_i, \\ \dot{I}_i^a &= \alpha \lambda_i(t) S_i - \gamma I_i^a, \\ \dot{I}_i^s &= \bar{\alpha} \lambda_i(t) S_i - \gamma I_i^s, \\ \dot{R}_i &= \gamma (I_i^a + I_i^s). \end{aligned} \quad (4)$$

The age structure of the population is specified the proportions N_i/N and the contact structure by the matrices C_{ij}^a and C_{ij}^s. We assume that symptomatic infectives reduce their contacts compared to asymptomatic infectives and set $C_{ij}^s = f^{sa} C_{ij}^a \equiv f^{sa} C_{ij}$, where $0 \leq f^{sa} \leq 1$ is the proportion by which this self-isolation takes place.

Social contact model: Partitioning contacts into spheres of home, workplace, school and all other categories, the contact matrix can be written as

$$C_{ij} = C_{ij}^H + C_{ij}^W + C_{ij}^S + C_{ij}^O. \quad (5)$$

The social contact matrix C_{ij} denotes the average number of contacts made per day by an individual in class i with an individual in class j. Clearly, the total number of contacts between group i to group j must equal the total number of contacts from group j to group i, and thus, for populations of fixed size the contact matrices obey the reciprocity relation $N_i C_{ij} = N_j C_{ji}$.

Social distancing model: We model large-scale social distancing measures by time-dependent controls $u^W(t)$, $u^S(t)$ and $u^O(t)$ imposed on the *non-household* contacts, leading to the time-dependent contact matrix

$$C_{ij}(t) = C_{ij}^H + u^W(t) C_{ij}^W + u^S(t) C_{ij}^S + u^O(t) C_{ij}^O. \quad (6)$$

This allows for each one of the possible social distancing measures to be implemented at different points in and for different durations. For a lockdown, corresponding to the elimination of all social contacts other than household ones, a single control function

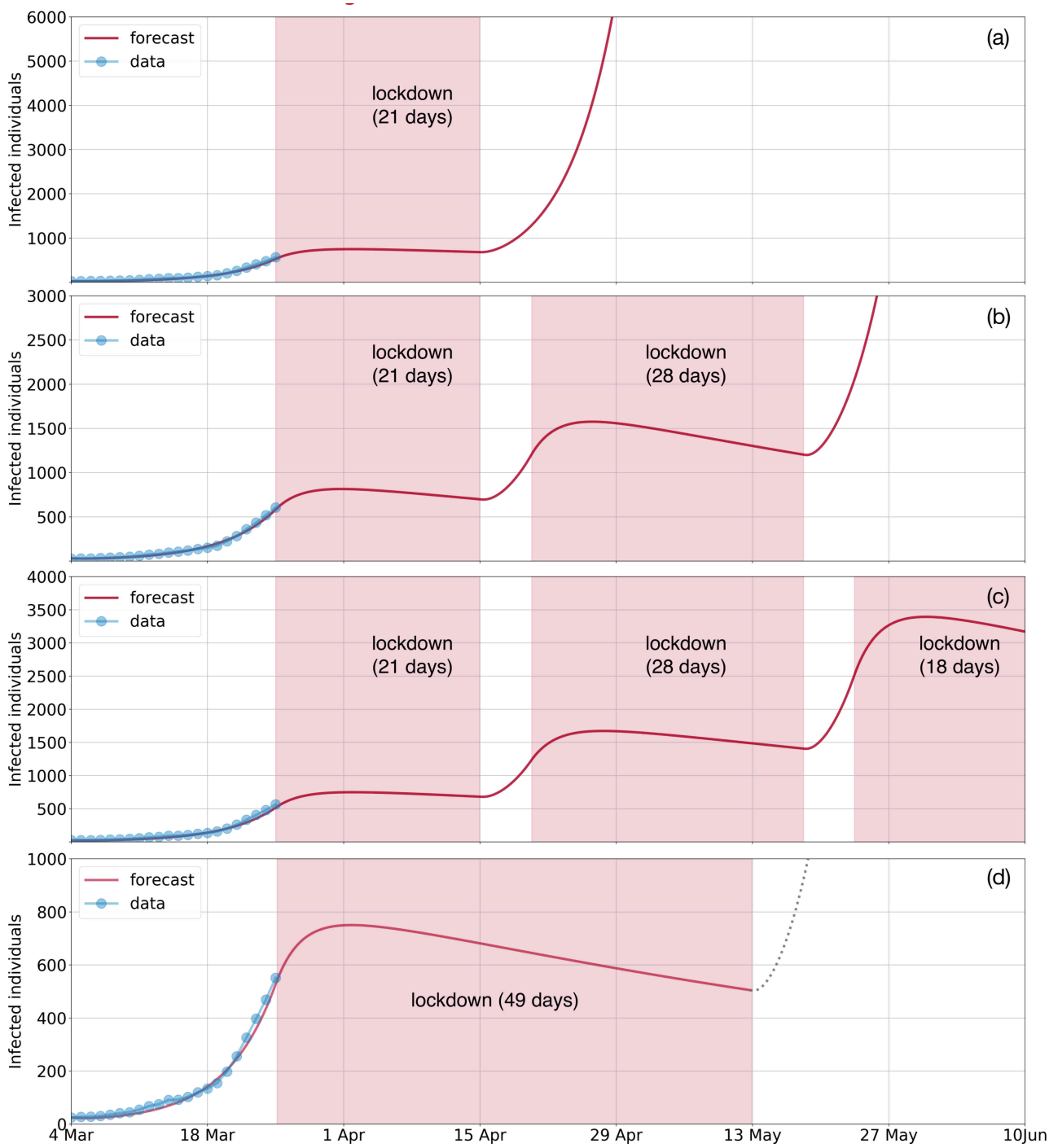

Figure 6. **Forecast of the COVID-19 epidemic in India with mitigatory social distancing using SEIR model.** Each of the four panels shows the variation in the number of infectives with lockdowns of various durations. The three-week lockdown starting 25th March does not prevent resurgence after its suspension as shown in panel (a). Neither does a further lockdown of 28 days spaced by a 5 day suspension, shown in panel (b). The protocols in panels (c) and (d), comprising of three lockdowns with 5 day relaxations and a single 49 day lockdown reduce case numbers below 10. This forecast is based on all cases being symptomatic so $\bar{\alpha} = 1$. The fit parameter is $\beta = 0.0315$, we set $\gamma = 1/7$ and $\gamma_E = 1/4$ [1].

$$2u(t) = -\tanh\left(\frac{t - t_{\rm on}}{t_w}\right) + \tanh\left(\frac{t - t_{\rm off}}{t_w}\right) \qquad (7)$$

is sufficient. Staggered social distancing measures can be constructed from linear combinations of these controls.

Basic reproductive ratio: We obtain the basic reproductive ratio by linearising the dynamics about the

disease-free fixed point, where $S_i = N_i$, and the evolution of infectives is governed by the $2M \times 2M$ linear stability matrix

$$\boldsymbol{J} = \gamma(\boldsymbol{L} - \boldsymbol{1}). \tag{8}$$

The $2M \times 2M$ *next generation* matrix

$$\boldsymbol{L} = \begin{pmatrix} \boldsymbol{L}^{aa} & \boldsymbol{L}^{as} \\ \boldsymbol{L}^{sa} & \boldsymbol{L}^{ss} \end{pmatrix}$$

consists of the $M \times M$ blocks

$$L^{aa}_{ij} = \frac{\alpha\beta}{\gamma} C^a_{ij} \frac{N_i}{N_j}, \quad L^{as}_{ij} = \frac{\alpha\beta}{\gamma} C^s_{ij} \frac{N_i}{N_j}, \tag{9}$$

$$L^{sa}_{ij} = \frac{\bar{\alpha}\beta}{\gamma} C^a_{ij} \frac{N_i}{N_j}, \quad L^{ss}_{ij} = \frac{\bar{\alpha}\beta}{\gamma} C^s_{ij} \frac{N_i}{N_j}, \tag{10}$$

and $\boldsymbol{1}$ is the $2M \times 2M$ identity matrix. Collecting both the asymptomatic and symptomatic infectives in the vector $\boldsymbol{I} = (\boldsymbol{I}^a, \boldsymbol{I}^s) = (I^a_1, \ldots, I^a_M, I^s_1, \ldots, I^s_M)$, their dynamics at early times is

$$\boldsymbol{I}(t) = \exp\left[\gamma(\boldsymbol{L} - \boldsymbol{1})t\right] \cdot \boldsymbol{I}(0). \tag{11}$$

Expressing $\boldsymbol{L}$ in its spectral basis of eigenvectors $\boldsymbol{V}$ and diagonal matrix of eigenvalues $\boldsymbol{\Lambda} = \mathrm{diag}(\Lambda_1, \ldots, \Lambda_{2M})$ we get $\exp\left[\gamma(\boldsymbol{L} - \boldsymbol{1})t\right] = \boldsymbol{V}\mathrm{diag}[\exp\gamma(\boldsymbol{\Lambda} - \boldsymbol{1})t]\boldsymbol{V}^{-1}$. For the epidemic to grow, it is sufficient for the spectral radius of $\boldsymbol{L}$ to be greater than unity. The basic reproductive ratio is defined to be the spectral radius of $\boldsymbol{L}$ [12]:

$$\mathcal{R}_0 \equiv \rho(\boldsymbol{L}) = \max\{|\Lambda_1|, \ldots, |\Lambda_{2M}|\}. \tag{12}$$

If eigenvalue with the largest magnitude is real, the basic reproductive ratio gives the most dominant contribution

$$\exp\left[\gamma(\mathcal{R}_0 - 1)t\right]$$

to the initial growth of the epidemic. This shows that the basic reproductive ratio depends on *(a)* the probability of infection on contact β; (b) the social contact structure encoded in the matrix C_{ij}; (c) the fraction of asymptomatic to symptomatic infectives α; and (d) the fraction by which symptomatic infectives self-isolate f, *i.e.* a combination of pathogen-specific, social, and individual factors. The linearisation above can be carried out at any point in time t by making the replacements $N_i \longrightarrow S_i(t)$ and $C_{ij} \longrightarrow C_{ij}(t)$ in the expression for $\boldsymbol{L}$, giving the time-dependent stability matrix $\boldsymbol{L}^{(t)}$. We may define the spectral radius of $\boldsymbol{L}^{(t)}$ as the effective time-dependent basic reproductive ratio

$$\mathcal{R}^{\mathrm{eff}}_0(t) \equiv \rho(\boldsymbol{L}^{(t)}) = \max\{|\Lambda^{(t)}_1|, \ldots, |\Lambda^{(t)}_{2M}|\} \tag{13}$$

The linearised dynamics gives the number of infectives at time $t + \delta t$ to be

$$\boldsymbol{I}(t + \delta t) = \exp\left[\gamma(\boldsymbol{L}^{(t)} - \boldsymbol{1})\delta t\right] \cdot \boldsymbol{I}(t). \tag{14}$$

The number of infectives will have a negative rate of growth if $\mathcal{R}^{\mathrm{eff}}_0(t)$ is reduced to below unity upon effecting the social distancing measures. Therefore, $\mathcal{R}^{\mathrm{eff}}_0(t)$ is diagnostic of the instantaneous efficacy of social distancing measures and can be computed from the eigenspectrum directly. Assuming controls are imposed and relaxed periodically and over durations short compared to intrinsic relaxation times, the progress of the epidemic can be described as a series of rising and (possibly) falling exponentials with dominant time scales determined by the spectral radii of $\boldsymbol{L}$ and $\boldsymbol{L}^{(t)}$. To a first approximation, the dynamics of the rise and fall of infections with the removal and application of social distancing is governed by a pair of exponentials. The rising time constant is $\gamma(\mathcal{R}_0 - 1)$ while the falling time constant is $\gamma(\mathcal{R}^{\mathrm{eff}}_0(t_{\mathrm{on}}) - 1)$. From Fig. (2)c it is clear that the spectral radii are approximately constant away from peak infection times and, therefore, the time-dependence of the $\mathcal{R}^{\mathrm{eff}}_0(t)$ can be neglected to first approximation.

APPENDIX B: MODEL SENSITIVITY

In this section we confirm that SIR model of previous section provides the best-case-scenario. Adding more details to the model such as allowing for incubation will only worsen the time needed for mitigation. The result in the main text uses the SIR model. This model does not include incubation. We have repeated the analysis by adding to the SIR model an exposed E_i compartment (to give an age-structured SEIR model) and we see, as expected, that the infectious number grows beyond the lockdown for the time scale of the incubation. The SEIR equation is given as

$$\begin{aligned} \dot{S}_i &= -\lambda_i(t) S_i, \\ \dot{E}_i &= \lambda_i(t) S_i - \gamma_E E_i, \\ \dot{I}^a_i &= \alpha\gamma_E E_i - \gamma I^a_i, \\ \dot{I}^s_i &= \bar{\alpha}\gamma_E E_i - \gamma I^s_i, \\ \dot{R}_i &= \gamma(I^a_i + I^s_i). \end{aligned} \tag{15}$$

We use the above equation to redo the results of Fig.(4) in the main text. The result is given in Figure (6).

APPENDIX C: SIMULATION AND DATA

Numerical integration: We choose $M = 16$ to correspond to the 16 age groups into which the contact matrix data is partitioned. The $3M = 48$ ordinary differential equations are then numerically integrated using the open source Python library PyRoss which is freely available on GitHub [13].

Data sources: The data of infected people is obtained from the website Worldometers [14]. Age distributions

are sourced from the Population Pyramid website [3] and social contact structures from the state-of-the-art compilation of Prem et. al. [2] obtained from surveys and Bayesian imputation.

* rs2004@cam.ac.uk
† ra413@cam.ac.uk

[1] N. M. Ferguson *et al.*, "Impact of non-pharmaceutical interventions (npis) to reduce covid-19 mortality and healthcare demand," London: Imperial College COVID-19 Response Team, March **16** (2020), 10.25561/77482.
[2] K. Prem, A. R. Cook, and M. Jit, "Projecting social contact matrices in 152 countries using contact surveys and demographic data," PLoS Comp. Bio **13**, e1005697 (2017).
[3] "https://www.populationpyramid.net/," ().
[4] Martin C. J. Bootsma and Neil M. Ferguson, "The effect of public health measures on the 1918 influenza pandemic in u.s. cities," Proc. Natl. Acad. Sci. **104**, 7588–7593 (2007).
[5] Richard J. Hatchett, Carter E. Mecher, and Marc Lipsitch, "Public health interventions and epidemic intensity during the 1918 influenza pandemic," Proc. Natl. Acad. Sci. **104**, 7582–7587 (2007).
[6] Lev Semenovich Pontryagin, *Mathematical theory of optimal processes* (Gordon and Breach, New York, 1986).
[7] G. E. P. Box, "Science and statistics," J. Am. Stat. Ass. **71**, 791–799 (1976).
[8] R. M. Anderson, B. Anderson, and R. M. May, *Infectious diseases of humans: dynamics and control* (Oxford university press, 1992).
[9] M. J. Keeling and P. Rohani, *Modeling infectious diseases in humans and animals* (Princeton University Press, 2011).
[10] S. Towers and Z. Feng, "Social contact patterns and control strategies for influenza in the elderly," Math. Biosci. **240**, 241–249 (2012).
[11] N. M. Ferguson *et al.*, "Strategies for mitigating an influenza pandemic," Nature **442**, 448–452 (2006).
[12] O. Diekmann, J. A. P. Heesterbeek, and M. G. Roberts, "The construction of next-generation matrices for compartmental epidemic models," J. Royal Soc. Int. **7**, 873–885 (2010).
[13] "https://github.com/rajeshrinet/pyross," ().
[14] "https://www.worldometers.info/coronavirus," .